ACS central science

Research Article

Cite This: ACS Cent. Sci. 2019, 5, 917−926

http://pubs.acs.org/journal/acscii

Design of Safe Nanotherapeutics for the Excretion of Excess Systemic Toxic Iron

Srinivas Abbina,[†,‡,∥] Usama Abbasi,[†,‡,∥] Arshdeep Gill,[‡,§] Kendrew Wong,[‡] Manu Thomas Kalathottukaren,[†,‡] and Jayachandran N. Kizhakkedathu*[,†,‡,§]

[†]Department of Pathology and Laboratory Medicine, [‡]Center for Blood Research and Life Sciences Institute, and [§]Department of Chemistry, University of British Columbia, Vancouver, British Columbia V6T 1Z3, Canada

Supporting Information

ABSTRACT: Chronic transfusion of red blood cells (RBCs) to patients with β-thalassemia, sickle cell disease, and other acquired anemic disorders generates significant amounts of bioactive iron deposits in the body. The inactivation and excretion of redox active iron(III) from the blood pool and organs are critical to prevent organ damage, and are the focus of iron chelation therapy (ICT) using low molecular weight Fe(III) specific chelators. However, the current ICT is suboptimal because of the short circulation time of chelators, toxicity, severe side effects, difficult regime of administration, and patient noncompliance. To address this issue, we have designed long circulating and biodegradable nanoconjugates with enhanced circulation time and well-defined biodegradability to improve iron excretion and avoid nonspecific organ accumulation. A series of iron chelating nanoconjugates were generated with deferoxamine (DFO) as the iron(III) specific chelator using polymer scaffolds containing structurally different acidic pH sensitive ketal groups. The type of degradation linkages used in the polymer scaffold significantly influenced the vascular residence time, biodistribution, and mode of excretion of chelators in mice. Remarkably, the conjugate, BGD-60 (140 kDa; R_h, 10.6 nm; cyclic ketal), exhibited the long circulation half-life ($t_{1/2\beta}$, 64 h), a 768-fold increase compared to DFO, and showed minimal polymer accumulation in major organs. The nanoconjugates were found to be nontoxic and excreted iron significantly better than DFO in iron overloaded mice. BGD-60 showed greater iron mobilization from plasma ($p = 0.0390$), spleen ($p < 0.0001$), and pancreas ($p < 0.0001$) whereas BDD-200 (340 kDa; R_h, 13.7 nm; linear ketal) mobilized iron significantly better from the spleen, liver, and pancreas ($p < 0.0001$, $p < 0.0001$, and $p < 0.0001$, respectively) compared to DFO at equivalent doses. The nanoconjugate's favorable long blood circulation time, biodegradability, and iron excretion profiles highlight their potential for future clinical translation.

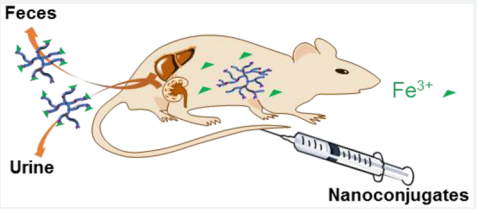

INTRODUCTION

Red blood cell (RBC) disorders such as thalassemia, sickle cell disease, Diamond−Blackfan anemia, aplastic anemia, and other acquired anemic disorders are becoming an important global health burden.[1] It is estimated that around 5−7% of the world population carries such traits, and ∼300 000−400 000 babies are born with inherited hemoglobin disorders each year.[1−3] Long-term RBC transfusions are the standard and widely used therapy to improve a patient's survival in these conditions.[4−6] In addition, conditions such as myelodysplastic syndromes (MDSs) require frequent RBC transfusions.[5] Although this is a lifesaving therapy, chronic RBC transfusions introduce a new clinical problem in the form of excess iron deposits in the body, termed as *transfusional iron overload* or *secondary iron overload*. Each unit of transfused RBC brings about 200 mg of iron into the body.[6] The excess iron supersaturates the iron storage capacity in plasma and in organs, and will be circulated as highly redox active, nontransferrin bound iron (NTBI) (Fe(III) form) as humans lack an iron excretion pathway. Over time, NTBI accumulates in the liver, heart, endocrine organs, and other tissues.[7] The free bioactive iron accumulation leads to the generation of reactive oxygen species (ROS), resulting in oxidative damage to lipids, proteins, DNA, and cellular organelles, such as lysosomes and mitochondria. This results in cellular dysfunction, apoptosis, necrosis, and fibrosis and ultimately leads to organ dysfunction that contributes to significant morbidity and mortality.[5,8−10] For example, cardiac and hepatic failures account for the major cause of death in β-thalassemia patients.[11−13] Significant iron overload also occurs in disease conditions such as hemochromatosis termed as *primary iron overload* because of the increased iron uptake from the gut and can cause severe organ dysfunction.

Iron chelation therapy (ICT) is the standard treatment in transfusional iron overload conditions using low molecular weight Fe(III) specific chelators that bind the excess bioactive iron and promote its clearance via the renal or hepatic pathway.[14] Deferoxamine (DFO), despite its poor oral availability, is the current gold standard in ICT. Although the other two oral chelators, deferiprone and deferasirox, showed an improved ease of use, they are far from an ideal candidate.[5] In addition, these chelators are associated with severe adverse side effects, such as hepatic and cardiac damage, neutropenia, gastrointestinal and neurotoxicity, agranulocyto-

Received: March 20, 2019
Published: April 11, 2019

DOI: 10.1021/acscentsci.9b00284
ACS Cent. Sci. 2019, 5, 917−926

A

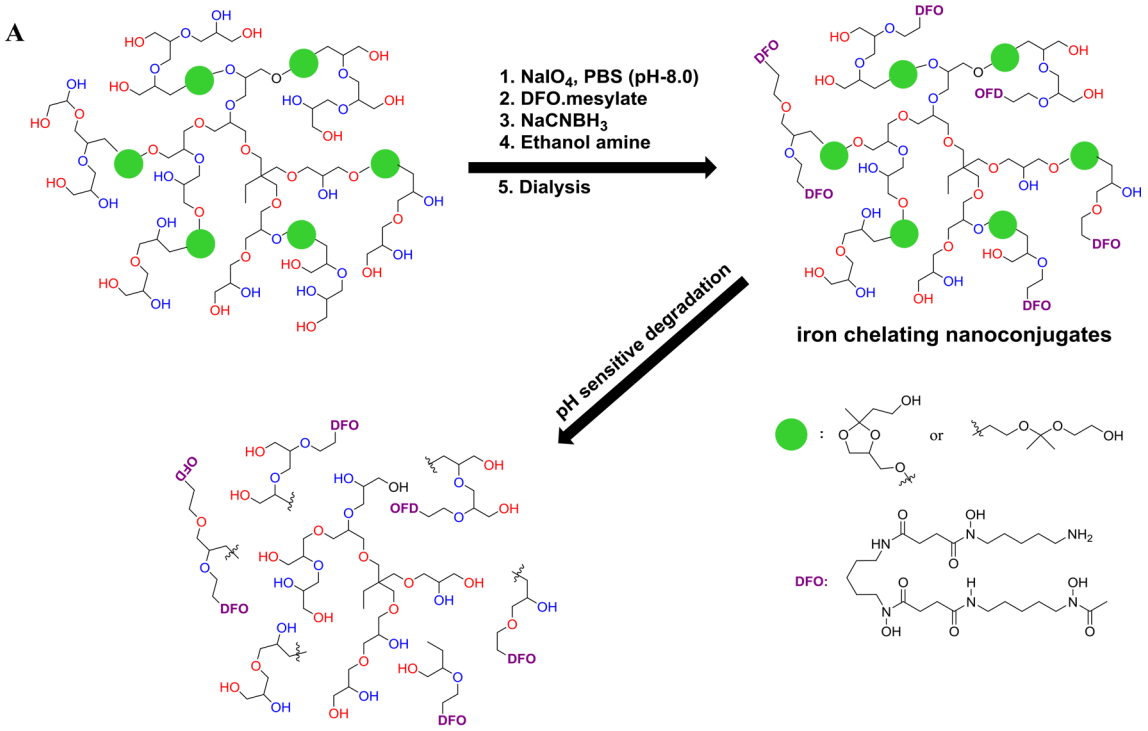

B

Iron chelating nanoconjugates	M_n of the BHPGs ($Đ$)[a]	M_n of the conjugates ($Đ$)[a]	R_h (nm)[b]	DFO/ conjugate[c]	DFO content (wt/wt)%[d]
BHPG-GHBKM-DFO15 (BGD-15)	86.4 (1.4)	98.1 (1.9)	7.7	16	10
BHPG-GHBKM-DFO30 (BGD-30)	86.4 (1.4)	132.5 (2.0)	9.4	32	21
BHPG-GHBKM-DFO60 (BGD-60)	86.4 (1.4)	141.0 (2.2)	10.6	60	39
BHPG-GHBKM-DFO110 (BGD-110)	86.4 (1.4)	182.5 (2.0)	13.0	120	77
BHPG-GHBKM-DFO220 (BGD-220)	260.0 (1.2)	384.0 (2.6)	19.6	220	48
BHPG-DMKM-DFO200 (BDD-200)	220.0 (1.3)	340.0 (1.7)	13.7	200	51

Figure 1. Synthesis and characterization of the biodegradable iron chelating nanoconjugates. (A) Synthetic scheme of biodegradable iron chelating nanoconjugates and its biodegradation. Structures of biodegradable groups incorporated within the polymer scaffold are shown. Deferoxamine (DFO) is used as an Fe(III) specific chelator (see also the Supporting Information). (B) Characteristics of the parent biodegradable hyperbranched polyglycerol (BHPG) and the corresponding nanoconjugates. (a) Absolute molecular weights (M_n, number-average molecular weight) of the polymers are determined by GPC-MALS. Polydispersity is given in parentheses. DMK incorporated BHPGs were labeled as BHPG-DMK, and GHBK incorporated BHPGs were listed BHPG-GHBK. (b) The hydrodynamic radius of the macrochelators was determined by quasielastic light scattering (QELS) analysis. (c) The number of DFO units was measured by UV−Vis spectroscopy. (d) Determined by thermogravimetry and UV−Vis spectroscopy.

sis, diarrhea, ophthalmic complications, growth retardation, and poor patient compliance, and are also very expensive.[5,15−19] As a result, investigations on safe, long-circulating, and more viable approaches would greatly benefit these patient groups.

Macromolecular conjugation has been widely known to mitigate the adverse effects of small molecular drugs and other potent agents such as aptamers.[20−24] In particular, conjugation of drugs with polymers offers significant advantages in terms of minimization of toxicity, enhancing circulation time, sustained release of drugs, biological activity, and solubility, among others.[25−29] For instance, dextran and hydroxyethyl starch (HES) conjugated DFOs showed promising results in improving vascular residence times and in minimizing adverse events of DFO in different clinical trials.[30,31] However, at times, achieving long circulation times is quite challenging;

DOI: 10.1021/acscentsci.9b00284
ACS Cent. Sci. 2019, 5, 917−926

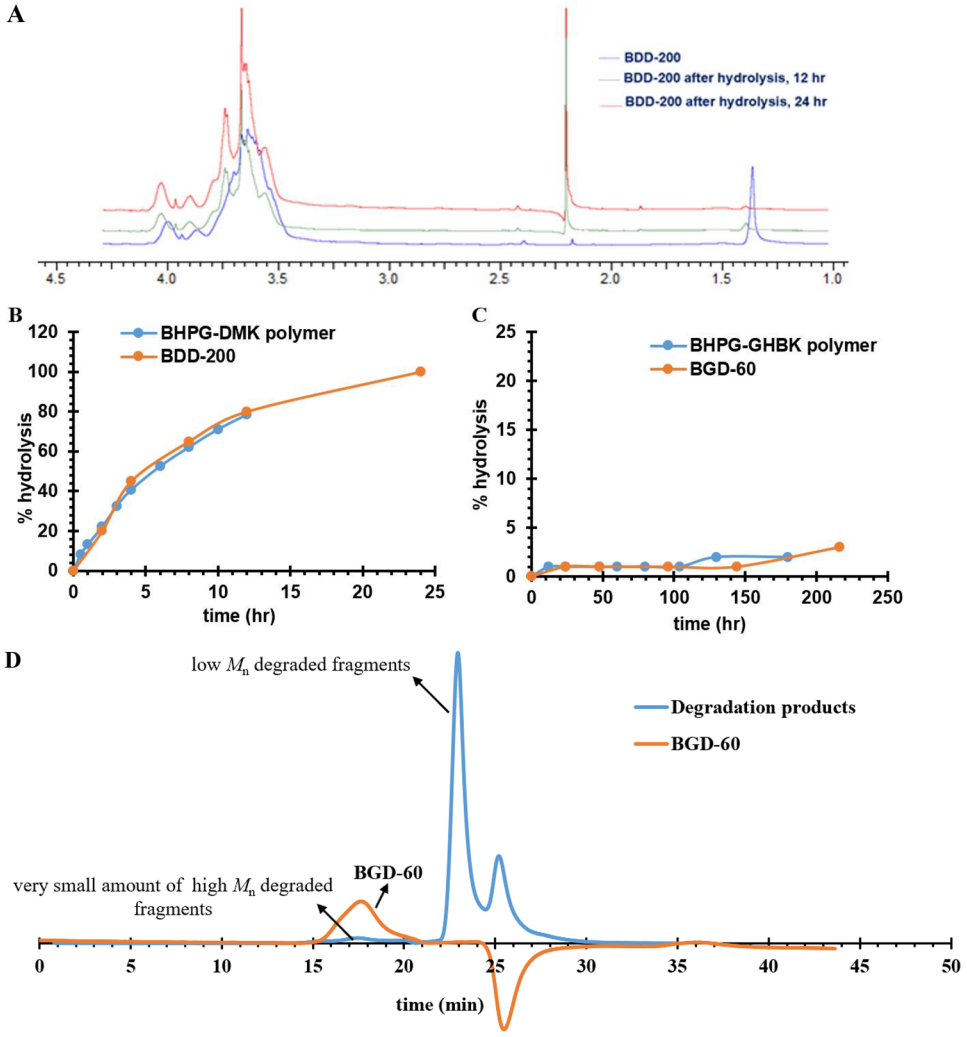

Figure 2. Degradation of biodegradable iron chelating nanoconjugates in deuterated water. (A) ^{1}H NMR spectra of nanoconjugates, BBD-220, and its degradation products measured at pH 7.4 and 37 °C. The new peak at 2.20 ppm corresponds to products formed upon degradation. Degradation kinetics of (B) BDD-200 and (C) BGD-60 at pH 7.4 at 37 °C measured by ^{1}H NMR analysis. The degradation pattern of the nanoconjugates was similar to that of the unconjugated polymer scaffold. (D) GPC traces of BGD-60 before and after degradation. BGD-60 was incubated in KCl/HCl (pH, 2.1) buffer for 20 h at 37 °C. The shift in the chromatogram confirms the degradation of BGD-60. The negative shift in the GPC trace of BGD-60 is due to a difference in the salt concentrations of the mobile phase and buffer used for sample preparation.

increased circulation times often lead to nonspecific organ accumulation, which is a major limitation of long-circulating polymer therapeutics as exemplified in the recent reports.[32−36] This is a potential challenge in the translation of these technologies, especially for chronic treatments. To avoid bioaccumulation, researchers used polymer scaffolds that have a molecular size lower than the kidney clearance limit;[37] however, this prevents the realization of long circulation. Thus, a biodegradable polymer design that generates longer blood circulation and stability without bioaccumulation could significantly increase the utilization of macromolecule-drug conjugation approaches.

In this article, we report the design and synthesis of a long-circulating, biodegradable iron chelating polymer nanotherapeutic, which shows efficient iron excretion and minimal nonspecific organ accumulation in mice. The degradation of the conjugate *in vivo* depends on the structure of ketal linkages used in the polymer scaffold. The current report is a first step in the generation of a long-acting and -circulating, biodegradable single molecule polymer nanotherapeutic with high iron excretion efficiency and minimal bioaccumulation.

RESULTS

Synthesis of Polymer Scaffold and DFO Nanoconjugates. We followed our recent report with a slight modification to generate a biodegradable scaffold for the iron chelating nanoconjugate synthesis (Schemes S1 and S2).[38,39] The macromolecular scaffold was generated by ring opening multibranching polymerization (ROMB) in a core−shell fashion. The acid cleavable ketal moiety incorporated biodegradable monomers, 2-(2-methyl-4-((oxiran-2-ylmethoxy)methyl)-1,3-dioxolan-2yl)ethanol (GHBK) and 2-(1-methyl-1-[2-(oxiran-2-ylmethoxy)ethoxy]ethoxy) ethanol (DMK), were copolymerized with glycidol to generate the degradable polymer core, and a shell layer of polyglycerol (Figure 1A) was incorporated around the core. The polyglycerol shell layer improved the solubility of the scaffold. The synthesis involves the polymerization of a mixture of biodegradable monomer and glycidol (1:1 molar ratio),

DOI: 10.1021/acscentsci.9b00284
ACS Cent. Sci. 2019, 5, 917−926

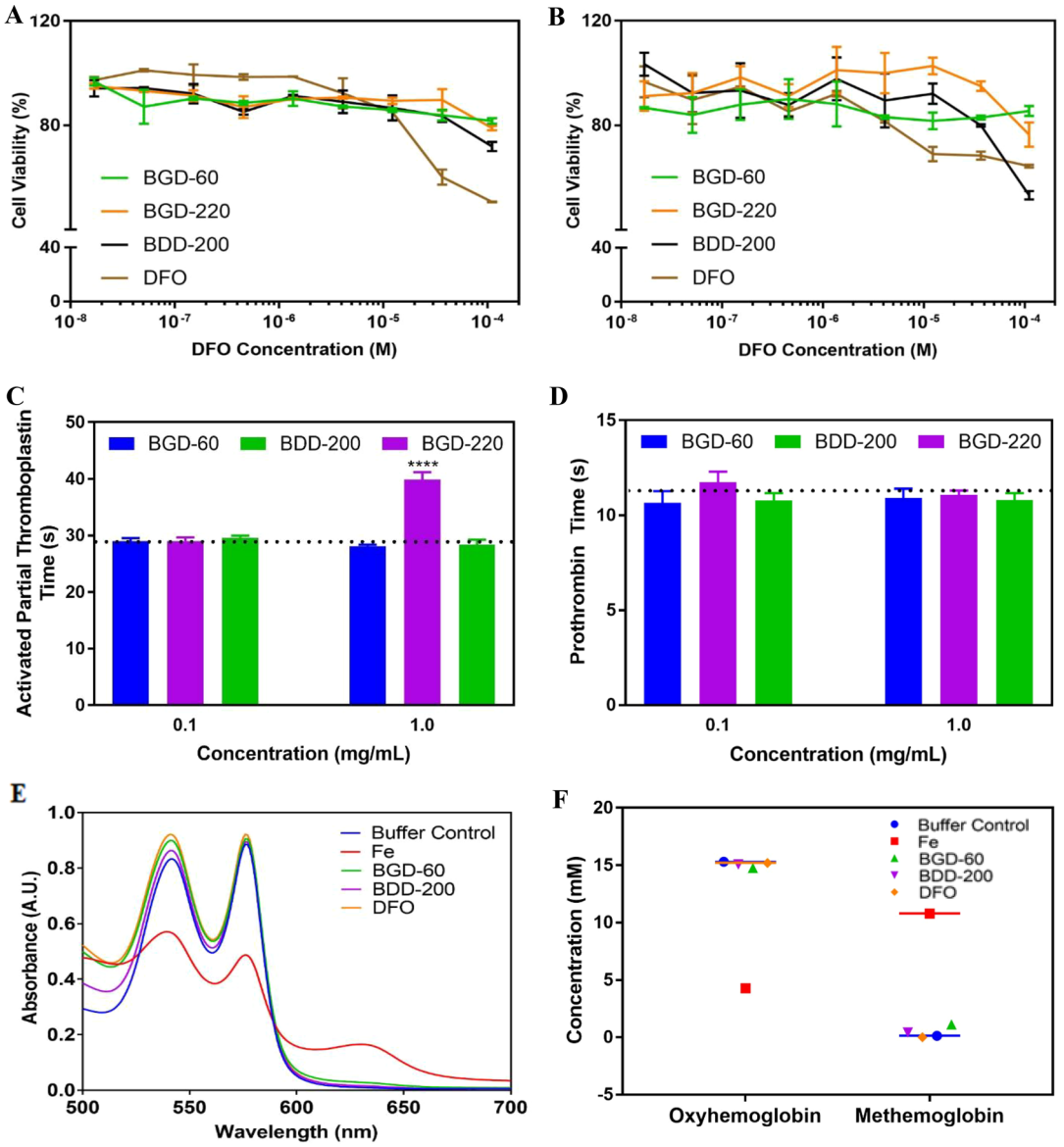

Figure 3. *In vitro* toxicity, blood compatibility, and activity of iron chelating nanoconjugates. Cell viability of (A) HepG2 and (B) fibroblast cells in the presence of nanoconjugates and DFO measured using the MTT assay. Influence of nanoconjugates on blood coagulation measured by (C) activated partial thromboplastin time (aPTT) and (D) prothrombin time (PT) ($N = 3$). The dotted line represents the clotting time for the buffer ($N = 3$). (E) Prevention of Fe(III) mediated toxicity to proteins by nanoconjugates and DFO. Hemoglobin is used as a model protein. (F) Quantification of formation of oxyhemoglobin and methemoglobin after treatments with DFO, buffer, Fe(III), and nanoconjugates.

initiated by partial deprotonated trimethylolpropane, over 24 h followed by polyglycerol shell synthesis through ROMB of glycidol in the same reaction mixture. The ketal monomer content of the polymers was limited to 13−15% to avoid any solubility issues in water and was confirmed by ^{1}H NMR analysis (Figures S1 and S3). The absolute molecular weights of the biodegradable hyperbranched polyglycerols (BHPGs) [BHPG-GHBK-1 (83 kDa; $Đ$, 1.4), BHPG-GHBK-2 (260 kDa; $Đ$, 1.4), and BHPG-DMK (220 kDa; $Đ$, 1.5)] were determined by gel permeation chromatography coupled with multiangle laser light scattering (GPC-MALS) (Figure 1B and Figure S5). The degree of branching of these BHPG variants was determined by ^{13}C inverse-gated NMR spectroscopy measurements (0.55−0.60) and was consistent with the low molecular weight BHPGs reported previously.[39]

A series of biodegradable DFO nanoconjugates were synthesized by a reductive amination approach with different DFO contents (Figure 1, Schemes S3 and S4). Aldehyde groups were generated on BHPG in a quantitative manner by treating it with $NaIO_4$ in buffer conditions and were conjugated with DFO. The excess aldehyde groups on BHPG were quenched with ethanolamine, purified by dialysis against buffer (pH, 11), and stored at 4 °C in solution. Conjugation of DFO to the polymer scaffold was confirmed by ^{1}H NMR analysis (Figures S2 and S4), and the absolute molecular weight and hydrodynamic radius (R_h) of the conjugates were determined by GPC-MALS (Figure 1B and Figure S5). A complete size distribution profile of the nanoconjugates in water was measured by dynamic light scattering (DLS) (Figure S6). The number of DFO units on BHPGs was determined by UV−Vis spectroscopy analysis (Figure 1B and Figure S7). The number of DFO units per conjugate were varied from 16 to 200 depending on the polymer molecular weight.

DOI: 10.1021/acscentsci.9b00284
ACS Cent. Sci. 2019, 5, 917−926

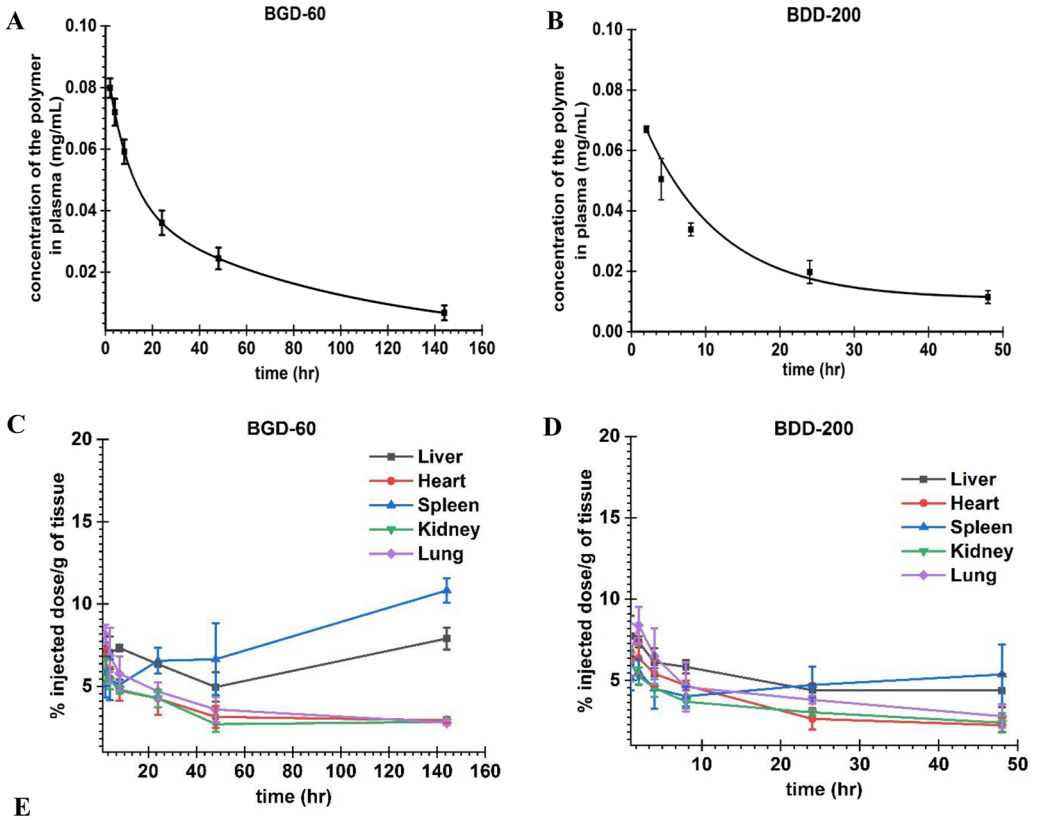

E

Iron chelating nanoconjugate	P_o (mg/mL) plasma	V_c (mL plasma)	α(h^{-1})	β(h^{-1})	$t_{1/2,\alpha}$ (h)	$t_{1/2,\beta}$ (h)	k_{12} (h^{-1})	k_2 (h^{-1})	k_{21} (h^{-1})	$AUC_{0-\infty}$ (mg/mL/hr)
BGD-60	0.093	0.103	0.104	0.011	6.69	64.3	0.038	0.020	0.056	4.67
BDD-200	0.065	0.147	0.107	0.087	6.488	7.930	0.001	0.097	0.097	0.099

P_o – initial volume dose, V_c – volume of the central compartment, $t_{1/2\beta}$ –circulation half-life time from elimination (β), $t_{1/2\alpha}$ –circulation half-life time from distribution (α), k_{12}, k_2, and k_{21} blood to tissue, elimination, and tissue to blood rate constants respectively, AUC (area under the curve)-exposure of the mice for the chelators.

F

	%injected dose/g of feces					%injected dose/g of urine			
time (h)	8	24	48	144	total	24	48	144	total
BGD-60	22.6	9.3	4.6	3.3	39.8	7	2	1.5	10.5
BDD-200	12.7	5.5	6.9	n.c	25.1	19.8	2.8	n.c	22.6

Figure 4. Vascular residence and biodistribution of biodegradable iron chelating nanoconjugates in mice with different degradation profiles. (A) Concentration of BGD-60 in the plasma (mg/mL) of mice at different time points. (B) Concentration of BDD-200 in the plasma (mg/mL) of mice at different time points. Female Balb/c mice (N = 4) were injected intravenously (via tail vein) with ^{3}H-labeled nanoconjugates, and the concentration was measured via scintillation counting. Shorter circulation of BDD-200 is made evident by its faster disappearance from plasma. (C, D) Biodistribution of BGD-60 and BDD-200. Organs (liver, heart, spleen, kidney, and lung) were collected at different time points, and the activities in the organs were measured and expressed as percent of injected dose (%ID). (E) Pharmacokinetic parameters of the nanoconjugates in mice (N = 4) obtained by fitting the concentration of nanoconjugates at different time points to a two-compartment model (origin 2018). Concentration in plasma, tissue volume, and all rate constants were derived, and error bars indicate standard deviations. (F) Excretion of nanoconjugates in urine and feces. BGD-60 selectively excreted through the hepatic pathway whereas BDD-200 did not show any preference.

***In Vitro* Degradation of Iron Chelating Nanoconjugates.** For an investigation of the effect of DFO conjugation on degradation of the conjugates and a comparison of their properties with the parent BHPG scaffold, two conjugates (BGD-60 and BDD-200) (Figure 1B) were chosen. The degradation kinetics of the conjugates was monitored by ^{1}H NMR spectroscopy in deuterated water (pH, 7.4) at 37 °C. The intensity of the ketal group's protons (1.35 ppm) that was decreased with the concurrent appearance of a new peak at 2.15−2.20 ppm on the ^{1}H NMR spectrum confirmed the degradation (Figure 2A). Intensity of the new peak at 2.15−2.20 ppm was used to quantify the degradation kinetics of the conjugates; the BDD-200 conjugate was degraded rapidly compared to BGD-60 (Figure 2B). The degradation half-life of the BDD-200 was almost 4.7 h. In contrast, no new peaks were noticed for BGD-60, and degradation was happening very slowly (Figure 2C). The degradation profiles of the nanoconjugates were almost similar to parent BHPG scaffolds. More importantly, since the two conjugates showed a different degradation profile, it offers a great advantage in altering the pharmacokinetics, excretion, bioaccumulation, and bioactivity. The size exclusion chromatography analysis of acidic KCl/HCl buffer (pH, 2.1; 37 °C; 20 h) incubated nanoconjugates (BGD-60 and BDD-200) showed a shift in refractive index

DOI: 10.1021/acscentsci.9b00284
ACS Cent. Sci. 2019, 5, 917−926

trace toward higher retention times, confirming further the degradation of nanoconjugates into very small fragments (Figure 2D and Figure S8). For further verification of the ketal controlled degradation of nanoconjugates and an estimation of their *in vitro* clearance, the KCl/HCl (pH, 2.1) buffer treated radio-labeled ($^3H_1$) nanoconjugates and controls were loaded in a dialysis cassette (MWCO-2 and 20 kDa) and dialyzed against water. The concentration of the nanoconjugates in the cassette was monitored over 72 h and compared with nondegradable HPG-DFO (Figure S9A). BGD-60 and BDD-200 were degraded into small fragments and diffused into water slowly. Only ∼10% of the nanoconjugate was left in the cassette for both degradable chelators whereas the control, HPG-DFO, was retained at almost 85% in the cassette. Most of the degraded nanoconjugates were cleared off (>98%) from the cassette with a cutoff of 20 kDa within 24 h (Figure S9B). This further validated the ketal groups in nanoconjugates are acid sensitive, degraded under an acidic environment, and promoting the clearance of nanoconjugates.

***In Vitro* Toxicity and Blood Compatibility of Nanoconjugates.** Although DFO has been clinically used in ICT for almost four decades, it is known for its antiproliferative and cytotoxic characteristics.[40] Thus, for an investigation of whether DFO conjugates can reduce the cytotoxicity in comparison to free DFO, the cell viability of human hepatocellular carcinoma cells (HepG2) and mouse fibroblasts (NIH/3T3 cell line) was investigated by MTT (3-(4,5-dimethylthiazol-2-yl)-2,5-diphenyltetrazolium bromide) assay. Cells were treated with either pure chelators [DFO, deferiprone (DFP), and deferasirox (DFX)], DFO conjugates at different concentrations (0−1 mM DFO equivalents), or media alone for 48 h. The conjugates were well-tolerated and showed good cell viability in the millimolar range of DFO equivalents when compared to DFO alone (Figure 3A,B, Figure S10). BGD-60 and BGD-110 showed good cell viability even at 1 mM DFO equivalent concentration in both fibroblasts (89% and 101%, $p = 0.0005$ and $p = 0.0001$, respectively) and HepG2 cells (73% and 83%, $p < 0.0001$ and $p < 0.0001$, respectively) (Figure 3A,B) in comparison to DFO. A similar tolerance profile was observed for other conjugates (Figure S10A,B) irrespective of their molecular weights. Further, the cell compatibility of the nanoconjugates was compared with FDA approved chelators including DFP and DFX and showed very high cell viability with nanoconjugates (Figure S10C,D). The reversal of free radical generation with nanoconjugates was examined in HepG2 cells loaded with iron (400 μM of iron from ferric ammonium citrate) using a fluorescent-based assay. A decreasing trend was observed for nanoconjugates relative to low molecular weight iron chelators (DFO, DFX, and DFP), although it is not significantly different (Figure S11).

Since the conjugates are going to be injected in blood and may circulate in blood after administration, we looked at the blood compatibility of these chelators. We utilized blood coagulation measurements [activated partial thromboplastin time (aPTT) and prothrombin time (PT)] in human plasma as an initial investigation. Figure 3C,D shows clotting times of the conjugates (1.0 and 0.1 mg/mL) in human plasma; values are reported as the average of three donors and in triplicate measurements per donor. With the exception of BGD-30 at 0.1 mg/mL and BGD-220 at 1.0 mg/mL, the clotting times of all nanoconjugates were comparable to that of the buffer control and were not influencing the blood coagulation (Figure S10D,F). Since the conjugates showed minimal influence on blood coagulation, and we extensively studied the blood compatibility of nonbiodegradable chelators[33,32] and the biodegradable polymer scaffold,[39] we did not perform those detailed studies here.

Prevention of Iron Mediated Oxidation of Proteins with Nanoconjugates. To assess the iron binding of the conjugates and, hence, the prevention of iron mediated oxidation of proteins *in vitro*, we used a model protein hemoglobin. The hemoglobin (HbA, ∼15 μM) from packed red blood cells (RBCs) showed two characteristic maximum absorbances in between 500 and 600 nm. The Fe(III) sulfate hydrate (100 μM) treated HbA showed a decrease in absorbance and showed a new peak around 635 nm, confirming the oxidation of oxyhemoglobin to methemoglobin (12 mM) (Figure 3E,F). The conjugates (BGD-60 and BDD-200) and DFO (equivalent DFO concentrations) treated HbA in the presence of Fe(III) sulfate did not form methemoglobin, and no change in oxyhemoglobin concentrations (15 mM) confirms the protection against iron mediated injury by the conjugates (Figure 3F).

Circulation Half-Life and Biodistribution of the Nanoconjugates. Two representative conjugates, BGD-60 and BDD-200, were chosen to investigate the blood circulation and biodistribution. These conjugates have different degradation profiles as discussed previously. The conjugates were radio-labeled ($^3H_1$) by the partial methylation of hydroxyl groups (∼1% of the hydroxyl groups) to form a stable methoxy group and were injected in Balb/c mice ($N = 4$) at a dose of 10 mg/kg. The concentration of conjugates in plasma as a function of time was determined by measuring the radioactivity at different time points (Figure 4A,B). The data (plasma concentration versus time) were fitted to a two-compartment model (using origin-2018 software) to determine pharmacokinetic parameters of the conjugates (Figure 4E). The circulation half-life ($t_{1/2\beta}$) of BGD-60 was 64 h which translates to a ∼768-fold higher value compared to DFO (Figure 4A). The circulation half-life of BDD-200 was 7.9 h (Figure 4B). With a change in the degradable linkages, the vascular residence time of conjugates was altered.

Next, we looked at the accumulation of conjugates in major organs including the liver, kidney, spleen, lung, and heart as well as its excretion through urine and feces at each time point. The bioaccumulation was quantified by radio-activity measurements. As shown, accumulation of the conjugates in organs is minimal for both of the tested conjugates which lies in between 2% and 11% irrespective of any time point (Figure 4C,D).

In the case of BGD-60, tissue accumulation is gradually decreased in most of the organs except for the liver and spleen (Figure 4C). The conjugate BDD-200 showed very minimal accumulation, which is around 2% in most of the organs except the liver which showed around 4% accumulation at 48 h (Figure 4D). BDD-200 showed less accumulation compared to BGD-60 possibly due to the faster degradation of BDD-200. We also measured the radioactivity of nanoconjugates in urine and feces to ensure that the degraded fragments of nanoconjugates are being excreted over time. The majority of the BGD-60 was excreted through the liver whereas BDD-200 did not show any preference (Figure 4F). Favorable long circulation and minimal bioaccumulation are important characteristics of these iron chelating conjugates.

Iron Excretion and Mobilization in Iron Overload Mice. Next, we looked at the efficiency of iron chelating

DOI: 10.1021/acscentsci.9b00284
ACS Cent. Sci. 2019, 5, 917−926

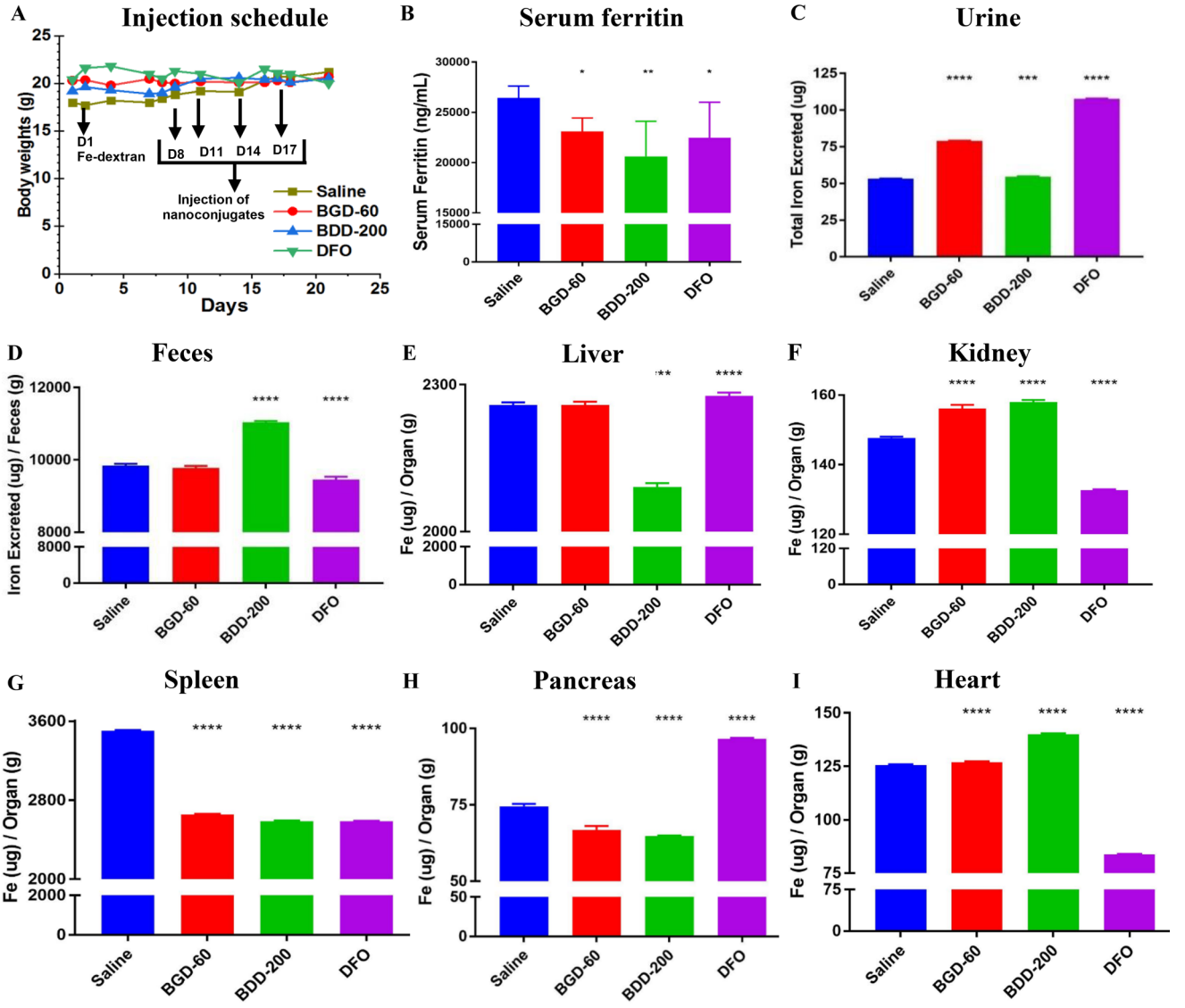

Figure 5. Iron excretion and mobilization by biodegradable iron chelating nanoconjugates in iron overloaded mice. (A) Dose schedule and mean body weight of the mice during the study. Iron overloaded mice (Balb/c) were prepared by administering Fe-dextran (150 mg/kg) on day 1. On day 8, mice were injected with nanoconjugates or DFO (100 mg/kg equivalent DFO) (N = 4 per group) intravenously (tail vein), followed by 3 injections on day 11, day 14, and day 17. One group of mice was injected with a similar volume of saline (200 μL) (N = 4). All the mice were sacrificed on day 21. Plasma, serum, and organs were collected. Urine and feces were collected using metabolic cages from day 8. (B) Serum ferritin levels (N = 4 per group) measured by colorimetric ELISA assay. Total iron excreted through (C) urine and (D) feces. Iron content in the samples was determined by inductively coupled plasma mass spectrometry. The total iron content in the organs: (E) liver, (F) kidney, (G) spleen, (H) pancreas, and (I) heart. Statistical significance have been indicated with asterisks as follows: **** represents $p < 0.0001$, *** $p = 0.002$, ** $p = 0.0014$, and * $p = 0.0215$. The error bars are for interassay replicates for four biological replicates (N = 4).

conjugates in excreting iron *in vivo* utilizing an iron overloaded mice model induced by injecting iron-dextran (day 1). The chelators (DFO and conjugates) were injected via the tail vein (100 mg/kg DFO or DFO equivalents) (4 injections) at different intervals (day 8, 11, 14, and 17). The body weight of the mouse increased during the experiments, and no drug related toxicity was observed (Figure 5A). Histological examination of the major organs (liver and kidney) further showed no abnormality or any appreciable necrosis in conjugate treated organs compared to controls (Figures S12 and S13). The serum and organs were collected at the end of the experiment on day 21. Urine and feces were collected throughout the experiment using metabolic cages.

The serum ferritin level is a very good biomarker to assess the NTBI in plasma in iron overload conditions. Figure 5B shows serum ferritin levels in iron overloaded mice treated with saline, BGD-60, BDD-200, and DFO. A significant decrease in serum ferritin levels is observed between BGD-60, BDD-200, and DFO treatments compared to the saline placebo (p = 0.039, p = 0.001, and p = 0.021, respectively.) There were no significant differences between the treatments, possibly because of the short duration of the study.

Further, for an investigation of the iron excretion efficacy of the conjugates, and a study of the influence of circulation time and biodegradability on iron mobilization from different organs, the iron content was measured using inductively coupled plasma mass spectrometry (ICP-MS). A significant increase in urinary iron excretion was observed for all treatments, BGD-60, BDD-200, and DFO, when compared to the saline control ($p < 0.0001$, p = 0.0002, and $p < 0.0001$,

DOI: 10.1021/acscentsci.9b00284
ACS Cent. Sci. 2019, 5, 917−926

respectively) (Figure 5C). Of importance, urine iron content was statistically the highest in DFO treatments, followed by BGD-60 ($p = 0.0012$) and then by BDD-200 ($p < 0.0001$ for all).

A significant increase in iron excretion was observed through the feces for iron overloaded mice treated with BDD-200 when compared to the saline control ($p < 0.0001$) and DFO ($p < 0.0001$) (Figure 5D); less iron is excreted via the feces in the DFO group ($p < 0.0001$). The iron content (μg) per organ (g) for major organs is shown in Figure 5E−I. BGD-60 significantly mobilized iron from the spleen and pancreas ($p < 0.0001$ and $p < 0.0001$, respectively) (Figure 5G,H). BDD-200 was able to mobilize iron from the spleen, liver, and pancreas ($p < 0.0001$, $p < 0.0001$, and $p < 0.0001$, respectively) compared to DFO (Figure 5G,E,H). In the heart, we did not notice any improvement with conjugates compared to DFO (Figure 5I). In the case of BDD-200, there is high iron content compared to the control; it might come from the Fe-dextran iron loaded mice model itself rather than being a result of the nanoconjugate treatment as we noticed a very small amount of BGD-200 accumulation in the heart (Figure 4D). Overall, we noticed the iron excretion via urine or feces dependent on the type of biodegradable linkages used. Also, the biodistribution is influencing the iron excretion; for instance, the long-circulating slowly degrading conjugate (BGD-60) needed more time for its excretion from the liver (Figure 5D). The quickly degrading iron chelating conjugate BDD-200 showed efficient iron excretion through the feces, and the liver iron content was much lower than in other treatment groups.

Safety Statement. For most of the chemicals used in the manuscript, no unusual safety precautions are expected except for NaH. Care should be taken by using dry apparatus and using it under inert atmosphere.

DISCUSSION

The landscape of polymer therapeutics including polymer conjugates is expanding rapidly, and a few recent successful clinical trials confirmed this steep progress.[41,42] In particular, the conjugation of small molecular drugs with macromolecules enhances the bioavailability and compatibility, minimizing the toxicity, and improving the efficiency and specificity of the drugs.[20,21] In the case of ICT, previous studies highlight the importance of polymer conjugation that dramatically increases the circulation time and decreases the toxicity.[32,33] However, the bioaccumulation of conjugates and the chemistry/biocompatibility of the polymer scaffold are two important determinants which affect the eventual clinical translation of these conjugation approaches. We anticipate that nontoxic polymer conjugates with longer plasma circulation times and minimal organ accumulation, and having controlled biodegradation, would be a front-runner in the race to generate an ideal therapeutic candidate for ICT.

Hyperbranched polyglycerol (HPG) and its biodegradable versions have been known for their biocompatibility and have been highlighted recently.[43,44] Biodegradability of these structures can be controlled by changing the acid cleavable ketal linkages without altering biocompatibility of the scaffold.[38] We utilized such polymer scaffolds to generate DFO conjugates to investigate the role of biodegradation on circulation time, bioaccumulation, and iron excretion.

We have chosen two different biodegradable polymer scaffolds with fast (BHPG-DMK) and slow (BHPG-GHBK) degradation profiles for this purpose. Our data clearly illustrated that circulation time and bioaccumulation can be dramatically changed by altering the degradation linkages within the polymer (Figure 4). Biodegradation of the nanoconjugate is vital in avoiding the nonspecific accumulation in organs for its utility in long-term iron mobilization and excretion without toxicity. The ketal groups used in the nanoconjugate's design are pH sensitive, and they degraded via hydrolysis into ketones and alcohols in an acidic environment.[45] The kinetics of hydrolysis of these ketals is highly dependent on the surrounding chemical framework. Our data show that the kinetics of degradation did not change upon conjugation with DFO *in vitro* and hydrolyzed into small molecular weight fragments under an acidic environment which can even be diffused through a 2 kDa cutoff dialysis cassette. However, in mice, DFO conjugation slightly decreased its degradation ability. This is evident from our recent data showing that BHPG-DMK and BHPG-GHBK without DFO have faster degradation in mice, evident by shorter blood circulation.[39,45] Thus, DFO conjugation slightly alters the scaffold properties *in vivo*. Although the degradation is slightly slowed, BHPG-DMK-based conjugates (BDD-200) showed minimal bioaccumulation and cleared from the body rapidly through both feces and urine. The BHPG-GHBK conjugate, BGD-60, showed slightly higher accumulation in the body due to the higher stability and consequent longer circulation. Interestingly, BGD-60 preferentially showed a hepatic excretion pathway. This suggests that the type of ketal linkage can influence the excretion pathway in mice. We anticipate that this bioaccumulation will further go down with time as demonstrated recently.[45] The BHPG-GHBK polymer without DFO almost completely excreted from mice within 30 days after the injection.[45]

One of the major limitations of the current FDA approved small molecule chelators is their toxicity. Although DFO is therapeutically effective, its infusions generate side effects in a dose dependent manner, and it has shown visual and auditory neurotoxicity due to chronic treatment. In addition, abdominal pain, nausea, and hypotension were observed after DFO administration.[46,47] The conjugation of DFO to a biodegradable scaffold dramatically increases its biocompatibility. In addition, the conjugation did not interfere with its ability to bind iron and protect against iron mediated toxicity. Since NTBI is known for its ability to damage different biomolecules by free radical mediated oxidation,[48] our data on the protection of proteins highlight its utility in preventing ROS generation *in vivo*. The DFO density and structural variance of nanoconjugates also did not show any influence on the oxidation of proteins.

Short vascular residence time is one of the major limitations of FDA approved Fe(III) chelators used in ICT.[4] For example, the gold standard DFO has a circulation half-life of about 20−30 min in humans and 5 min in mice. Because of the rapid elimination, DFO is administered for long time periods in either intravenous or subcutaneous modes. DFO is infused 7 h/day for 5−6 days a week.[6] Conjugation of DFO to macromolecules can alter the circulation times, and few examples are shown in the literature.[29−32,35,36] Our slowly degrading nanoconjugates generated ultralong circulation with $t_{1/2}$ around 64 h in mice. The quickly degrading conjugate has a circulation time around 7.9 h in mice which is also considerably higher than DFO. Our studies further demonstrated that the newly developed conjugates show efficient iron excretion profiles, and the iron excretion can be modulated by

DOI: 10.1021/acscentsci.9b00284
ACS Cent. Sci. 2019, 5, 917−926

changing the biodegradable linkages within the polymer scaffold. Interestingly, conjugates, in particular BDD-200, are more efficient in mobilization of iron from the liver compared to the kidney. This might be due to the exclusive hepatic pathway of elimination for BHPG-DMK polymer[39] and possibly its conjugates. Together our data support the fact that the biodegradable conjugates are nontoxic and efficient in sequestration of iron from different organs as well as plasma in iron overloaded mice without accumulation in the body.

CONCLUSIONS

In summary, we have developed a series of long-acting and biodegradable iron chelating nanoconjugates by conjugating DFO with different biodegradable polymer scaffolds. The conjugates were well-characterized by NMR spectroscopy, UV−Vis spectroscopy, and gel permeation chromatography, and these are found to be less toxic compared to DFO and were able to prevent iron mediated oxidation of proteins. The conjugate, BGD-60, showed very long circulation in mice, which is 768-fold higher than that of DFO. Importantly, bioaccumulation and iron mobilization of these new conjugates are modulated by changing the cleavable linkages within the polymer scaffold. In general, the conjugates showed very low accumulation in major organs and are highly efficient in iron excretion. Long-term iron efficacy studies would be needed to further evaluate the iron excretion efficacy of these chelators, and these studies are in progress.

ASSOCIATED CONTENT

Supporting Information

The Supporting Information is available free of charge on the ACS Publications website at DOI: 10.1021/acscentsci.9b00284.

All methods, additional data, and figures including synthetic schemes, ^{1}H NMR spectra, GPC traces, DLS chromatograms, UV−Vis spectroscopy traces, *in vitro* diffusion−clearance profiles, cell viability studies, cellular ROS generation, and photomicrographs (PDF)

AUTHOR INFORMATION

Corresponding Author

*E-mail: jay@pathology.ubc.ca. Phone: 1-604-822-7085. Fax: 1-604-822-7742.

ORCID

Srinivas Abbina: 0000-0002-9103-7444

Manu Thomas Kalathottukaren: 0000-0001-5374-7114

Jayachandran N. Kizhakkedathu: 0000-0001-7688-7574

Author Contributions

‖S.A. and U.A. contributed equally to this work.

Notes

The authors declare no competing financial interest.

ACKNOWLEDGMENTS

The authors acknowledge the funding by Canadian Institutes of Health Research (CIHR) and Canada Foundation for Innovation (CFI). The authors thank the Macromolecular Hub, CBR, for the use of their research facilities and also thank Drs. Marcel Bally and Nancy Dos Santos for help with animal studies at British Columbia Cancer Research Centre. J.N.K. holds a Career Investigator Scholar award from the Michael Smith Foundation for Health Research (MSFHR). S.A. acknowledges an MSFHR postdoctoral fellowship. U.A. acknowledges a graduate scholarship from Centre for Blood Research. A.G. acknowledges funding from the NSERC CREATE NanoMat Program. K.W. acknowledges an Undergraduate Student Research Award (USRA) from NSERC.

REFERENCES

(1) Weatherall, D. J. The Inherited Diseases of Hemoglobin Are an Emerging Global Health Burden. *Blood* **2010**, *115* (22), 4331−4336.

(2) Weatherall, D. J.; Clegg, J. B. Inherited Haemoglobin Disorders: An Increasing Global Health Problem. *Bull. World Health Organ.* **2001**, *79* (8), 704−712.

(3) Weatherall, D. J. The Challenge of Haemoglobinopathies in Resource-Poor Countries. *Br. J. Haematol.* **2011**, *154* (6), 736−744.

(4) Brittenham, G. M. Iron-Chelating Therapy for Transfusional Iron Overload. *N. Engl. J. Med.* **2011**, *364* (15), 1475−1477.

(5) Sheth, S. Iron Chelation: An Update. *Curr. Opin. Hematol.* **2014**, *21*, 179−85.

(6) Poggiali, E.; Cassinerio, E.; Zanaboni, L.; Cappellini, M. D. An Update on Iron Chelation Therapy. *Blood Transfus.* **2012**, *10* (4), 411−422.

(7) Porter, J. B.; De Witte, T.; Domenica Cappellini, M.; Gattermann, N. New Insights into Transfusion-Related Iron Toxicity: Implications for the Oncologist. *Crit. Rev. Oncol.* **2016**, *99*, 261−271.

(8) Porter, J.; Viprakasit, V.; Kattamis, A. *Iron Overload and Chelation*, 3rd ed.; Cappellini, M. D., Cohen, A., Porter, J., Ali Taher, V. V., Eds.; Thalassaemia International Federation, 2014.

(9) Mobarra, N.; Shanaki, M.; Ehteram, H.; Nasiri, H.; Sahmani, M.; Saeidi, M.; Goudarzi, M.; Pourkarim, H.; Azad, M. A Review on Iron Chelators in Treatment of Iron Overload Syndromes. *Int. J. Hematol. Stem Cell Res.* **2016**, *10* (4), 239−247.

(10) Kontoghiorghes, G. J.; Kolnagou, A.; Peng, C.-T.; Shah, S. V.; Aessopos, A. Safety Issues of Iron Chelation Therapy in Patients with Normal Range Iron Stores Including Thalassaemia, Neurodegenerative, Renal and Infectious Diseases. *Expert Opin. Drug Saf.* **2010**, *9* (2), 201−206.

(11) Kremastinos, D. T.; Farmakis, D.; Aessopos, A.; Hahalis, G.; Hamodraka, E.; Tsiapras, D.; Keren, A. Beta-Thalassemia Cardiomyopathy: History, Present Considerations, and Future Perspectives. *Circ.: Heart Failure* **2010**, *3* (3), 451−458.

(12) Olivieri, N. F.; Liu, P. P.; Sher, G. D.; Daly, P. A.; Greig, P. D.; McCusker, P. J.; Collins, A. F.; Francombe, W. H.; Templeton, D. M.; Butany, J. Combined Liver and Heart Transplantation for End-Stage Iron-Induced Organ Failure in an Adult with Homozygous Beta-Thalassemia. *N. Engl. J. Med.* **1994**, *330* (16), 1125−1127.

(13) Wood, J. C. Diagnosis and Management of Transfusion Iron Overload: The Role of Imaging. *Am. J. Hematol.* **2007**, *82* (S12), 1132−1135.

(14) Kalinowski, D. S.; Richardson, D. R. The Evolution of Iron Chelators for the Treatment of Iron Overload Disease and Cancer. *Pharmacol. Rev.* **2005**, *57* (4), 547−583.

(15) Hamilton, J. L.; Hatef, A.; Imran Ul-Haq, M.; Nair, N.; Unniappan, S. Clinically Approved Iron Chelators Influence Zebrafish Mortality, Hatching Morphology and Cardiac Function. *PLoS One* **2014**, *9* (10), 109880.

(16) Simon, S.; Athanasiov, P. A.; Gilhotra, J. S.; Jain, R.; Raymond, G. Desferrioxamine-Related Ocular Toxicity: A Case Report. *Indian J. Ophthalmol.* **2012**, *60*, 315−317.

(17) Tenenbein, M.; Kowalski, S.; Sienko, A.; Bowden, D. H.; Adamson, I. Y. R.; Tenenbein, M. Pulmonary Toxic Effects of Continuous Desferrioxamine Administration in Acute Iron Poisoning. *Lancet* **1992**, *339* (8795), 699−701.

(18) Porter, J. B.; Huehns, E. R. The Toxic Effects of Desferrioxamine. *Bailliere's Clin. Haematol.* **1989**, *2* (2), 459−474.

(19) Olivieri, N. F.; Buncic, J. R.; Chew, E.; Gallant, T.; Harrison, R. V.; Keenan, N.; Logan, W.; Mitchell, D.; Ricci, G.; Skarf, B.; et al. Visual and Auditory Neurotoxicity in Patients Receiving Subcuta-

neous Deferoxamine Infusions. *N. Engl. J. Med.* **1986**, *314* (14), 869−873.
(20) Duncan, R. The Dawning Era of Polymer Therapeutics. *Nat. Rev. Drug Discovery* **2003**, *2*, 347−360.
(21) Kopeček, J. Polymer−drug Conjugates: Origins, Progress to Date and Future Directions. *Adv. Drug Delivery Rev.* **2013**, *65* (1), 49−59.
(22) Larson, N.; Ghandehari, H. Polymeric Conjugates for Drug Delivery. *Chem. Mater.* **2012**, *24* (5), 840−853.
(23) Pelegri-O'Day, E. M.; Lin, E.-W.; Maynard, H. D. Therapeutic Protein−Polymer Conjugates: Advancing Beyond PEGylation. *J. Am. Chem. Soc.* **2014**, *136* (41), 14323−14332.
(24) Shu, J. Y.; Panganiban, B.; Xu, T. Peptide-Polymer Conjugates: From Fundamental Science to Application. *Annu. Rev. Phys. Chem.* **2013**, *64* (1), 631−657.
(25) Yang, J.; Kopeček, J. Macromolecular Therapeutics. *J. Controlled Release* **2014**, *190*, 288−303.
(26) Greish, K.; Fang, J.; Inutsuka, T.; Nagamitsu, A.; Maeda, H. Macromolecular Therapeutics. *Clin. Pharmacokinet.* **2003**, *42* (13), 1089−1105.
(27) Danhier, F.; Ansorena, E.; Silva, J. M.; Coco, R.; Le Breton, A.; Préat, V. PLGA-Based Nanoparticles: An Overview of Biomedical Applications. *J. Controlled Release* **2012**, *161* (2), 505−522.
(28) Sun, H.; Hong, Y.; Xi, Y.; Zou, Y.; Gao, J.; Du, J. Synthesis, Self-Assembly, and Biomedical Applications of Antimicrobial Peptide−Polymer Conjugates. *Biomacromolecules* **2018**, *19* (6), 1701−1720.
(29) Hallaway, P. E.; Eaton, J. W.; Panter, S. S.; Hedlund, B. E. Modulation of Deferoxamine Toxicity and Clearance by Covalent Attachment to Biocompatible Polymers. *Proc. Natl. Acad. Sci. U. S. A.* **1989**, *86* (24), 10108−10112.
(30) Harmatz, P.; Grady, R. W.; Dragsten, P.; Vichinsky, E.; Giardina, P.; Madden, J.; Jeng, M.; Miller, B.; Hanson, G.; Hedlund, B. Phase Ib Clinical Trial of Starch-Conjugated Deferoxamine (40SD02): A Novel Long-Acting Iron Chelator. *Br. J. Haematol.* **2007**, *138* (3), 374−381.
(31) Dragsten, P. R.; Hallaway, P. E.; Hanson, G. J.; Berger, A. E.; Bernard, B.; Hedlund, B. E. First Human Studies with a High-Molecular-Weight Iron Chelator. *J. Lab. Clin. Med.* **2000**, *135* (1), 57−65.
(32) Imran Ul-Haq, M.; Hamilton, J. L.; Lai, B. F. L.; Shenoi, R. A.; Horte, S.; Constantinescu, I.; Leitch, H. A.; Kizhakkedathu, J. N. Design of Long Circulating Nontoxic Dendritic Polymers for the Removal of Iron in Vivo. *ACS Nano* **2013**, *7* (12), 10704−10716.
(33) Hamilton, J. L.; Imran ul-haq, M.; Abbina, S.; Kalathottukaren, M. T.; Lai, B. F. L.; Hatef, A.; Unniappan, S.; Kizhakkedathu, J. N. In Vivo Efficacy, Toxicity and Biodistribution of Ultra-Long Circulating Desferrioxamine Based Polymeric Iron Chelator. *Biomaterials* **2016**, *102*, 58−71.
(34) Qian, J.; Sullivan, B. P.; Peterson, S. J.; Berkland, C. Nonabsorbable Iron Binding Polymers Prevent Dietary Iron Absorption for the Treatment of Iron Overload. *ACS Macro Lett.* **2017**, *6* (4), 350−353.
(35) Liu, Z.; Lin, T.-M.; Purro, M.; Xiong, M. P. Enzymatically Biodegradable Polyrotaxane−Deferoxamine Conjugates for Iron Chelation. *ACS Appl. Mater. Interfaces* **2016**, *8* (39), 25788−25797.
(36) Liu, Z.; Qiao, J.; Nagy, T.; Xiong, M. P. ROS-Triggered Degradable Iron-Chelating Nanogels: Safely Improving Iron Elimination in Vivo. *J. Controlled Release* **2018**, *283*, 84−93.
(37) Alexis, F.; Pridgen, E.; Molnar, L. K.; Farokhzad, O. C. Factors Affecting the Clearance and Biodistribution of Polymeric Nanoparticles. *Mol. Pharmaceutics* **2008**, *5* (4), 505−515.
(38) Shenoi, R. A.; Narayanannair, J. K.; Hamilton, J. L.; Lai, B. F. L.; Horte, S.; Kainthan, R. K.; Varghese, J. P.; Rajeev, K. G.; Manoharan, M.; Kizhakkedathu, J. N. Branched Multifunctional Polyether Polyketals: Variation of Ketal Group Structure Enables Unprecedented Control over Polymer Degradation in Solution and within Cells. *J. Am. Chem. Soc.* **2012**, *134* (36), 14945−14957.
(39) Shenoi, R. A.; Lai, B. F. L.; Imran ul-haq, M.; Brooks, D. E.; Kizhakkedathu, J. N. Biodegradable Polyglycerols with Randomly Distributed Ketal Groups as Multi-Functional Drug Delivery Systems. *Biomaterials* **2013**, *34* (25), 6068−6081.
(40) Lee, Y. S.; Wurster, R. D. Deferoxamine-Induced Cytotoxicity in Human Neuronal Cell Lines: Protection by Free Radical Scavengers. *Toxicol. Lett.* **1995**, *78* (1), 67−71.
(41) Duncan, R. Polymer Therapeutics: Top 10 Selling Pharmaceuticals — What Next? *J. Controlled Release* **2014**, *190*, 371−380.
(42) Atkinson, S.; Andreu, Z.; Vicent, M. Polymer Therapeutics: Biomarkers and New Approaches for Personalized Cancer Treatment. *J. Pers. Med.* **2018**, *8* (1), 6.
(43) Abbina, S.; Vappala, S.; Kumar, P.; Siren, E. M. J.; La, C. C.; Abbasi, U.; Brooks, D. E.; Kizhakkedathu, J. N. Hyperbranched Polyglycerols: Recent Advances in Synthesis, Biocompatibility and Biomedical Applications. *J. Mater. Chem. B* **2017**, *5* (47), 9249−9277.
(44) Wilms, D.; Stiriba, S.-E.; Frey, H. Hyperbranched Polyglycerols: From the Controlled Synthesis of Biocompatible Polyether Polyols to Multipurpose Applications. *Acc. Chem. Res.* **2010**, *43* (1), 129−141.
(45) Shenoi, R. A.; Abbina, S.; Kizhakkedathu, J. N. *In Vivo* Biological Evaluation of High Molecular Weight Multifunctional Acid-Degradable Polymeric Drug Carriers with Structurally Different Ketals. *Biomacromolecules* **2016**, *17* (11), 3683−3693.
(46) Cui, H.-J.; He, H.; Yang, A.-L.; Zhou, H.-J.; Wang, C.; Luo, J.-K.; Lin, Y.; Tang, T. Efficacy of Deferoxamine in Animal Models of Intracerebral Hemorrhage: A Systematic Review and Stratified Meta-Analysis. *PLoS One* **2015**, *10* (5), e0127256.
(47) Arandi, N.; Haghpanah, S.; Safaei, S.; Zahedi, Z.; Ashrafi, A.; Eatemadfar, P.; Zarei, T.; Radwan, A. H.; Taher, A. T.; Karimi, M. Combination Therapy - Deferasirox and Deferoxamine - in Thalassemia Major Patients in Emerging Countries with Limited Resources. *Transfus. Med.* **2015**, *25* (1), 8−12.
(48) Welch, K. D.; Davis, T. Z.; Van Eden, M. E.; Aust, S. D. Deleterious Iron-Mediated Oxidation of Biomolecules. *Free Radical Biol. Med.* **2002**, *32* (7), 577−583.

DOI: 10.1021/acscentsci.9b00284
ACS Cent. Sci. 2019, 5, 917−926